Sensors & Actuators: B. Chemical 389 (2023) 133920

Contents lists available at ScienceDirect

Sensors and Actuators: B. Chemical

journal homepage: www.elsevier.com/locate/snb

Multichannel microfluidic virus sensor for rapid detection of respiratory viruses using virus-imprinted polymer for digital livestock farming

Raufur Rahman Khan [a], Hussam Ibrahim [a], Gaurav Rawal [b], Jianqiang Zhang [b], Meng Lu [a,c], Liang Dong [a,d,*]

[a] Department of Electrical & Computer Engineering, Iowa State University, Ames, IA, USA
[b] Department of Veterinary Diagnostic & Production Animal Medicine, Iowa State University, Ames, IA, USA
[c] Department of Mechanical Engineering, Iowa State University, Ames, IA, USA
[d] Microelectronics Research Center, Iowa State University, Ames, IA, USA

ARTICLE INFO

Keywords:
Virus imprinted polymer
Microfluidics
Swine flu virus sensor
Digital agriculture

ABSTRACT

This paper reports a multichannel microfluidic sensor for detecting H1N1 swine influenza A virus (IAV). This device integrates six independent sensing elements, measurement chambers, and passive mixers on a microfluidic platform to enable parallel processing and analysis of multiple samples. The sensing element uses a conducting virus-imprinted polymer (VIP) to recognize, immobilize, and qualify the target H1N1 virus. The VIP is formed via electropolymerization of 2-amino-1,3,4-thiadiazole monomers and template H1N1 virus particles and subsequent removal of the template particles. The formed cavities are complementary to H1N1 virus in shape and size. High selectivity, conductance, and charge transfer characteristics make the VIP suitable for electrochemical detection of H1N1 virus. The sensor demonstrates a linear response to the logarithmic concentration of H1N1 virus in a concentration range of up to 5×10^6 TCID50/mL with a limit of detection of 9 TCID50/mL. The sensor exhibits high selectivity to H1N1 virus in the presence of several non-specific swine pathogens. Further, the sensor can be regenerated and reused by simply washing the sensing surface with acetic acid. The device demonstrates parallel detection of H1N1 virus in nasal swabs, oral fluids, and lung homogenates sampled from swine with low consumption of reagents and samples.
Data Availability: Data will be made available on request

1. Introduction

Low-cost digital sensor technologies for livestock welfare and disease assessment help rapidly monitor animal health status, identify pathogens/agents, and develop interventions [1,2]. Viral pathogens are one of the major limiting factors to the productivity of swine industry [3]. Influenza A virus (IAV) infects swine, birds, humans, and other mammals. The subtype H1N1 influenza virus has threatened public health by causing severe pandemics [4]. The influenza pandemic in 1918 resulted in the deaths of 50–100 million people worldwide; the most recent one in 2009 led to severe damages with estimated socioeconomic losses of 55 billion USD [5]. Conventional methods for identifying and quantifying influenza viruses include reverse transcription-polymerase chain reaction (RT-PCR) [6], enzyme-linked immunoassays [7,8], immunoblotting [9], and immunofluorescence assays [10]. These methods provide high sensitivity and selectivity but are expensive, labor-intensive, and time-consuming and require skilled operators [11].

Recent advancements in biosensors and assays have led to rapid, low-cost, and portable solutions to detect viral particles without lysis [12]. For example, surface plasmon resonance, giant magnetoresistance, impedance, and electrochemical sensors have been demonstrated to detect viral particles [13–16]. Among these portable sensors, electrochemical virus sensors can offer high sensitivity and accuracy, where receptor molecules (e.g., peptide aptamer [17,18] and antibody [19]) are immobilized on the sensor surface to recognize target viruses. These sensors, however, still require relatively expensive reagents (e.g., antigen, antibody, aptamer) and have low reusability. Significant efforts have been made to develop molecularly imprinted polymer (MIP) technology as an economical solution to detect biomolecules [20,21]. Generally, MIPs are created by self-assembling monomers around a target molecule template. After the removal of the template, cavities are formed in the polymer and exhibit specificity to the target molecule [22,

* Corresponding author at: Department of Electrical & Computer Engineering, Iowa State University, Ames, IA, USA.
E-mail address: ldong@iastate.edu (L. Dong).

https://doi.org/10.1016/j.snb.2023.133920
Received 9 January 2023; Received in revised form 19 March 2023; Accepted 2 May 2023
Available online 3 May 2023

23]. The MIPs that can immobilize viral particles have been incorporated with the quartz crystal microbalance technique for virus detection with high sensitivity [24,25]. Non-conducting gel polymers and graphene oxide were combined to design MIP-based electrochemical sensors for rapid detection of Zika virus, showing high electrochemical responsivity [26]. Recently, several conducting polymers, such as poly (3,4-ethylene dioxythiophene), have been employed as the host polymer of MIPs that offer high electrical conductivity [27–29]. Despite the remarkable progress in developing MIP biosensors [30–34], research and development of MIP-based virus sensors are still in their infancy.

This paper reports a multichannel microfluidic sensor for rapidly detecting H1N1 influenza virus using a conducting virus-imprinted polymer (VIP). The device integrates an array of electrochemical virus-sensing elements into a microfluidic platform to test multiple samples simultaneously (Fig. 1a). Each sensing element is placed inside a measurement chamber downstream from a serpentine microfluidic passive mixer [35]. The sample and the redox electrolyte solution are infused into the mixer through the inlets of the microfluidic device. The sensing element is submersed in the mixed sample-electrolyte mixture (Fig. 1b). The VIP is formed on the surface of a patterned thin-film gold (Au) electrode via the electropolymerization of 2-amino-1,3,4-thiadiazole (ATD) monomers and H1N1 virus particles. The virus particles are a template embedded inside the polymer matrix of poly(ATD). After removing the virus template by washing the sensing surface with an etchant, specific cavities complementary to H1N1 virus particles are formed (inset of Fig. 1c, and Fig. 1d). These cavities are formed to match the shape and size of the target virus particle, thus serving as the specific binding sites. The underlying principle employed in this methodology is that the virus particles present in the analyte will conform to the configuration of the fabricated cavities and subsequently attach to them. Electrochemical impedance spectroscopy is adopted to quantify the target virus particles bound to the cavities. It is noted that the ATD monomers are electron deficient that can facilitate electron transfer by absorbing more electrons upon a chemical reaction; therefore, poly (ATD) can provide high conductance and excellent charge transfer characteristics [36]. To our knowledge, the ATD monomers have not yet been reported to form VIPs that are specific to target virus particles, while parallel processing and analysis of multiple samples with VIP-based virus sensors are rarely demonstrated.

2. Materials and methods

2.1. Materials

A solution of ATD monomers (Sigma-Aldrich, St. Louis, MO, USA) was prepared by adding 20 mM of ATD in a 100 mM H_2SO_4 solution. An acetic acid aqueous solution (10 % v/v) was prepared to remove the template of virus particles. For electrochemical characterization, 50 mM of potassium ferricyanide ($K_3[Fe(CN)_6]$) with 10 mM Na_2SO_4 was used as the redox electrolyte. Acetic acid, H_2SO_4, $K_3[Fe(CN)_6]$, $K_4[Fe(CN)_6]$, and Na_2SO_4 were purchased from Thermo Fisher Scientific (Pittsburgh, PA, USA).

2.2. H1N1 IAV isolate, other swine viral and bacterial pathogens, and swine clinical samples

The IAV isolate A/swine/MO/A01203163/2012 (H1N1) was isolated, propagated, and titrated in MDCK cells (ATCC CCL-34) following the previously published protocol [38]. This IAV isolate stock had an infectious titer of 10^7 median tissue culture infectious dose per mL (TCID50/mL). When making serial dilutions of the virus isolates, a minimum essential medium (MEM) was used. Swine viral and bacterial pathogens used in this study to evaluate the specificity of IAV H1N1 sensor include influenza B virus (IBV), influenza D virus (IDV), porcine reproductive and respiratory syndrome virus (PRRSV), porcine circovirus 2d (PCV2d), porcine hemagglutinating encephalomyelitis virus (PHEV), porcine respiratory coronavirus (PRCV), pseudorabies virus, *Glaesserella* (*Haemophilus*) *parasuis*, and *Mycoplasma hyopneumoniae*. Six swine oral fluids, nasal swabs, and lung tissue homogenates were selected from the samples submitted to Iowa State University Veterinary Diagnostic Laboratory. The samples were tested by IAV RT-qPCR (quantitative reverse transcription PCR) to verify their status.

2.3. Nucleic acid extraction and IAV PCR testing

Nucleic acids were extracted from 100 μL virus isolates or swine

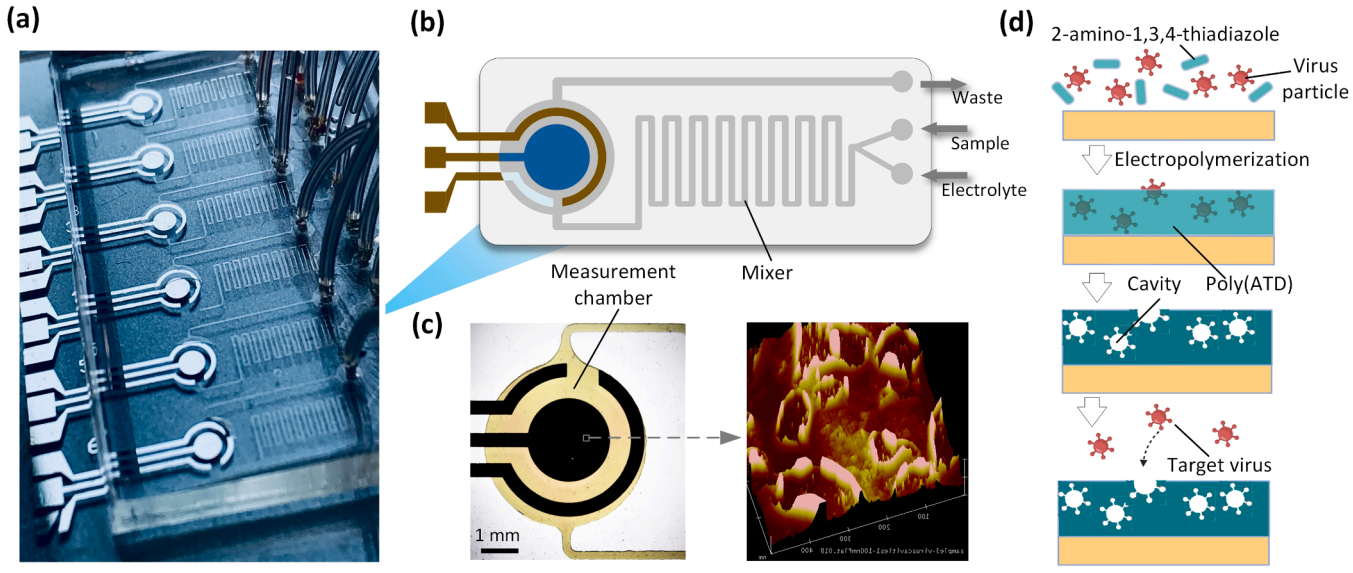

Fig. 1. (a) Optical image of a multichannel microfluidic virus detection device that integrates six VIP-based electrochemical sensing elements for parallel tests of virus. (b) Schematic of a microfluidic setup that integrates with an electrochemical sensing element, a passive mixer, two inlets, and one outlet. The working electrode of the sensing element is modified with the VIP. The waste exits the device through the outlet. (c) Optical image of a single electrochemical sensing element. The inset shows an atomic force microscopy image of the working electrode that contains the VIP with the cavities specific to H1N1 virus. (d) Schematic of synthesizing the VIP layer using 2-amino-1,3,4-thiadizole as the monomer and H1N1 virus particles as the template.

clinical samples using a MagMAX Pathogen RNA/DNA extraction kit (Thermo Fisher Scientific, Waltham, MA) and a Kingfisher Flex instrument (Thermo Fisher Scientific) according to the instructions of the kit manufacturer. Nucleic acids were eluted with 90 μL of elution buffer. For PCR testing, a commercial IAV RT-qPCR kit targeting conserved matrix gene and/or nucleoprotein gene (VetMAX-Gold SIV One-Step RT-PCR assay, Thermo Fisher Scientific) was used, and the previously described procedures were followed [39]. Cyclic threshold (Ct) values from the PCR test of serially diluted virus isolates (10^7, 10^6, 10^5, 10^4, 10^3, 10^2 TCID50/mL) were obtained. Samples with Ct < 38 were considered positive, and samples with Ct ≥ 38 were considered negative for IAV.

2.4. Fabrication of sensing elements

To fabricate the electrochemical sensing elements (Fig. 2a), a 5 nm-thick titanium (Ti) layer and a 100 nm-thick Au layer were sequentially deposited on the surface of a 100 nm-thick thermal oxide (SiO_2) layer grown on a silicon (Si) wafer by e-beam evaporation. The Au-Ti layers were then patterned to form the base electrodes of the working, counter, and reference electrodes (WE, CE, and RE, respectively) for the sensing elements using photolithography and subsequent wet etching. Next, 500 nm-thick Ag/AgCl paste was screen-printed at the surface of the RE. Subsequently, the Au-based WE (diameter: 2.5 mm) was modified with a seed layer of poly(ATD) by the first-time electrodeposition of ATD monomers with cyclic voltammetry (CV; CHI 760E electrochemical workstation). The seed layer of poly(ATD), with a thickness of 14 ± 1.5 μm, could not only aid in depositing the virus template containing poly(ATD), but also contribute to the structural strength of the VIP layer, even after the virus template has been removed. In this step, the ATD monomer solution (12 μL volume) was dropped on the sensor surface to cover all three electrodes; ten cycles of CV were then applied to deposit poly(ATD) in a potential range of 0–1.6 volts versus the Ag/AgCl pseudo-reference electrode at the scan rate of 100 mV/s. The electrodeposition of poly(ATD) was indicated by an increase in oxidation peak current around 1.4 V (Fig. 2b). After the seed poly(ATD) layer was deposited, a mixture of the prepared ATD monomer solution and the IAV H1N1 stock solution (10^7 TCID50/mL) at a 1:1 vol ratio was loaded on the electrodes, followed by another ten cycles of CV (Fig. 2c). This second-time electrodeposition resulted in the embedding of IAV H1N1 virus particles inside the polymer matrix of poly(ATD) that had a thickness of 13.5 ± 1.8 μm (Fig. 2d). According to the CV scans for electrodeposition (Fig. 2b, c), it was observed that the peak oxidation current increased as the number of cycles increased. However, after the 10th CV scan, the increase in peak oxidation current became almost negligible, suggesting that the degree of polymerization had reached its optimum level. For forming the cavities that could recognize the target virus (Fig. 2e), the polymer was washed with a 10 % (v/v) aqueous acetic acid solution accompanied by stirring with the help of a magnetic bar for 30 min [26]. To ensure the complete removal of residual acetic acid from the polymer matrix, the temperature of the DI water was increased to 50 °C. However, rinsing at room temperature for a minimum of 60 min was also effective. Moreover, it is worth noting that the virus template embedded internally may pose a challenge to be entirely removed. However, the polymer's porous characteristics may allow for the removal of the embedded virus templates to a certain extent during the removal process, although this may be difficult to confirm. Further, control devices were fabricated using the same approach described above, except adding no virus particles during the second-time electrodeposition. The control device is referred to as the non-VIP (NIP) device.

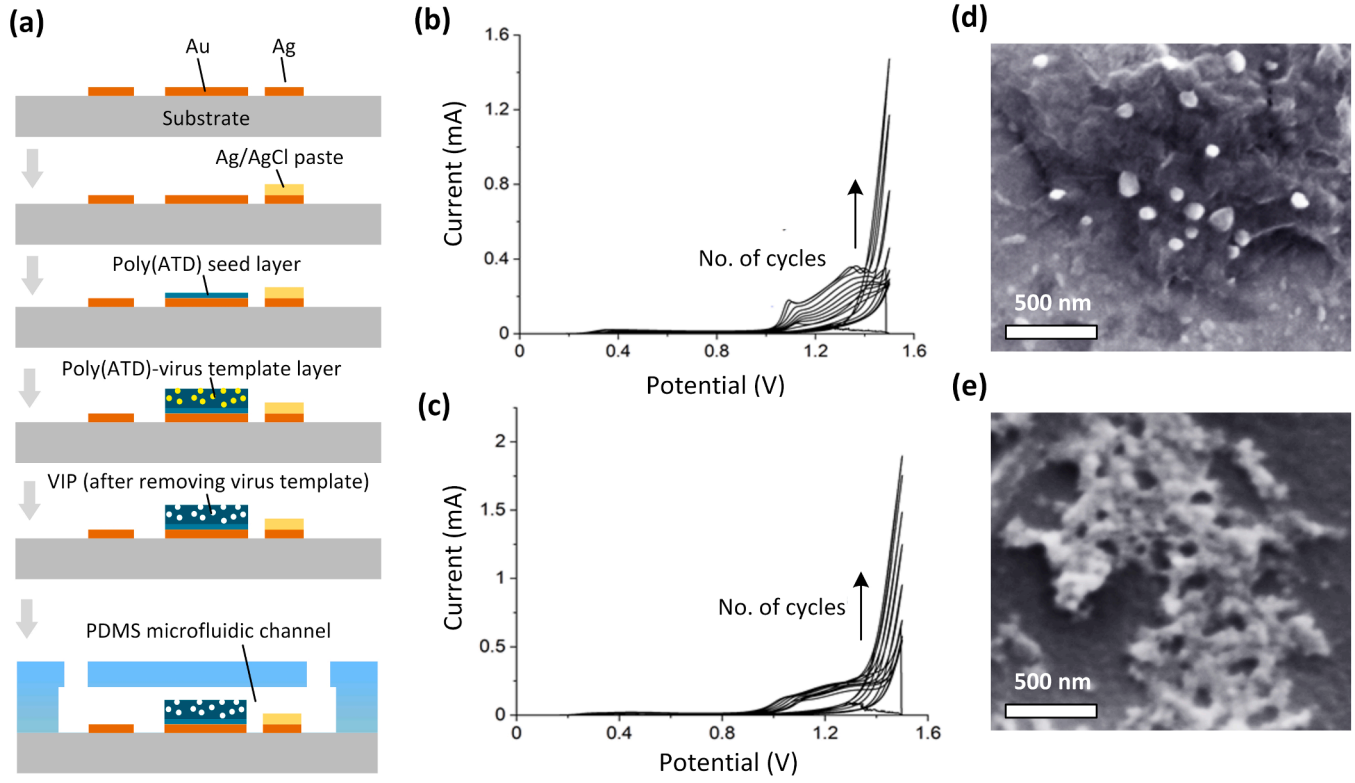

Fig. 2. (a) Schematic of the process flow for fabricating the microfluidic virus sensor. (b) CV for the first-time electropolymerization of the ATD monomer to form a seed layer of poly(ATD). (c) CV for the second-time electropolymerization of the ATD monomer and H1N1 virus to form a layer of poly(ATD)-virus complex. In both (b) and (c), the CV scan was conducted in a 0.1 M H_2SO_4 solution over a potential range from 0–1.6 volts at the scan rate of 100 mV/s. (d) Scanning electron microscopy (SEM) image of the poly(ATD) embedded with H1N1 virus particles. (e) SEM image for the VIP with cavities formed after the acetic acid wash and subsequent DI water cleaning.

2.5. Microfluidic chip fabrication

The multichannel microfluidic device was designed to realize the parallel detection of H1N1 IAV in multiple samples. The microfluidic channels were formed by bonding polydimethylsiloxane (PDMS) on the Si/SiO_2 substrate that contained the sensing elements. The width and height of the channels were 150 μm and 50 μm, respectively. The total length of the mixer region was 82 mm. The diameter of the measurement chamber was 5 mm. To form the channels, the photoresist of SU-8 2050 (50 μm thickness; Kayaku Advanced Materials) was spin-coated and patterned using UV lithography to create a master mold. Subsequently, the silicone elastomer base and curing agent (SYLGARD 184) were mixed in a weight ratio of 10:1 and degassed for 40 min. The mixed PDMS solution was poured over the master mold and cured at 70 °C for 90 min. After demolding, the PDMS channels were bonded to the substrate containing multiple sensing elements with the help of oxygen plasma treatment [40].

2.6. Operation of microfluidic chip

The multichannel microfluidic device integrated six independent microfluidic units, each comprising a VIP-based electrochemical sensing element specific to H1N1, a measurement chamber, a passive mixer, two inlets, and an outlet. One inlet was designated for the sample solution while the other was for the redox electrolyte solution. A programmable syringe pump (Model: NE-1200; ALA Scientific Instruments, Farmingdale, NY, USA), which could hold 12 sterile syringes (BD Luer-Lok™ 1-mL syringe, Mississauga, ON, Canada), was used to drive six samples and six redox electrolyte solutions simultaneously into the passive mixer via the inlets at a volumetric flow rate of 500 uL/hr. The 5 mm-diameter mixer was comprised of a serpentine channel with 32 turns to ensure thorough mixing of the two fluids. The electrochemical virus sensor was immersed in the mixed solution inside the circular measurement chamber, which was incubated for one minute before the EIS measurement was conducted for an additional minute. After the measurement, the waste fluid was discharged into an external waste bottle through the outlet.

2.7. Electrochemical impedance spectroscopy (EIS) measurement

The sensor utilized the EIS technique (CHI-760E electrochemical workstation) for the electrochemical detection of the target virus. First, to calibrate the sensor, the H1N1 stock virus solution (10^7 TCID50/mL titer) was diluted from 2 to 200,000 times with appropriate amounts of electrolyte solution that contained 50 mM of $[Fe(CN)_6]^{3-/4-}$ and 10 mM Na_2SO_4 as the redox probe and the supporting electrolyte, respectively. For the EIS measurement, a 12 μL of the diluted solution was loaded onto the sensing element. After the incubation for one minute, the EIS technique was applied with a frequency range from 100 kHz to 1 Hz, which took another minute to complete the measurement. The total time required for the incubation and EIS measurement was about 2 min. The value of charge transfer resistance R_{ct} was extracted by fitting the Nyquist plot. It should be noted that further increasing the incubation time had almost no effect on the value of R_{ct}.

3. Results and discussion

The SEM images shown in Fig. 2c indicate that H1N1 virus particles were conjugated with poly(ATD) through the electropolymerization process and that the cavities were formed after the removal of the H1N1 virus template from poly(ATD) with acetic acid (Fig. 2d). To examine changes in electrochemical properties of the working electrode during forming the VIP, both the CV and EIS techniques were applied to characterize the electrodes formed with different material compositions. These electrodes include (i) a bare Au electrode, (ii) an Au electrode modified with the seed poly(ATD) layer (namely, Au/poly(ATD)); (iii) an Au electrode containing both the seed poly(ATD) layer and the poly (ATD) layer embedded with H1N1 virus template (namely, Au/poly (ATD)/virus); and (iv) a final VIP electrode after the removal of the virus template (namely, Au/poly(ATD)/cavity). The CV result (Fig. 3a) indicates that the poly(ATD) could facilitate electron charge transfer, as evident by the increase of the oxidation peak current from 51 μA for the bare Au electrode to 125 μA for the Au/poly(ATD) electrode. Essentially, the extended p-orbital system of poly(ATD) can help prompt electron transfer from one end to the other end of this polymer, thus enhancing the electrocatalytic properties of the poly(ATD)-modified electrode [34]. More specifically, poly (ATD) is classified as a conjugated polymer, which is characterized by a backbone structure consisting of alternating single and double bonds. This unique structure features unstable π bonds that create an extended p-orbital system, enabling charge carriers to move throughout the polymer from one end to the other. This delocalization of charges is essential for the efficient transport of charges within a conducting polymer. The direction of conductivity is dependent on the molecular packing, which is facilitated by an extended p-orbital overlap, and enables electron transfer through intermolecular bonds. Therefore, the extended p-orbital system is the driving force for enhancing electron transfer and electrocatalytic properties of the polymer [36,37]. With the virus particles embedded into the polymer matrix, the peak oxidation current of the Au/poly(ATD)/virus electrode decreased to 53 μA, which may be associated with an increase in poly(ATD) thickness after the second-time electrodeposition. When the virus particles were washed away with acetic acid, the peak oxidation current of the Au/poly (ATD)/cavity electrode increased to 85 μA. In addition, a scan rate analysis was performed on the Au/poly(ATD)/cavity electrode using the CV technique over the scan rate range from 10 to 200 mV/s (Fig. 3c). The anodic peak current was found to increase linearly with the square root of scan rate (Fig. 3d), indicating that the Au/poly(ATD)/cavity electrode exhibited a diffusion-controlled process [41].

Next, EIS studies were performed to examine the charge-transfer resistance of the Au, Au/poly(ATD), Au/poly(ATD)/virus, Au/poly (ATD)/cavity electrodes (Fig. 3b). The value of R_{ct} for each electrode was extracted from the obtained Nyquist plot. The inset of Fig. 3b shows the equivalent circuit model consisting of the solution resistance (R_s), charge transfer resistance (R_{ct}), double layer capacitance (C_{dl}), and Warburg impedance (W), which was used to fit the EIS spectra [42]. After the seed poly(ATD) layer was deposited on the Au surface, the R_{ct} value decreased from 30.2 MΩ of the bare Au electrode to 431.2 kΩ. Embedding the virus particles into poly(ATD) caused a decrease of R_{ct} to 84.8 kΩ, and removing the virus particles from the polymer matrix increased R_{ct} to 185.2 kΩ.

To characterize the VIP-based virus sensor, the stock solution of H1N1 virus (10^7 TCID50/mL concentration) was diluted in the electrolyte solution (50 mM $[Fe(CN)_6]^{3-/4-}$ with 10 mM Na_2SO_4) to obtain a range of concentrations from 50 to 5×10^6 TCID50/mL. Fig. 4a shows the Nyquist plots obtained from the EIS measurement for these diluted virus samples. The result indicates that the value of R_{ct} decreased with increasing concentration of H1N1 virus (Fig. 4b). It is speculated that when interacting with the cavities, H1N1 virus particles, being negatively charged particles [26], may give electrons to the VIP, thus lowering the R_{ct} value of the electrode. The relative change in charge transfer resistance ΔR_{ct} of the sensor from the baseline $R_{ct,base}$ was calculated as $(R_{ct} - R_{ct,base})/R_{ct,base} = \Delta R_{ct}/R_{ct,base}$, where $R_{ct,base}$ was established by the EIS measurement for the pure redox electrolyte. The value of $\Delta R_{ct}/R_{ct,base}$ exhibited a linear response to the logarithmic concentration of H1N1 virus over the whole concentration range (Fig. 4b). The sensitivity of $\Delta R_{ct}/R_{ct,base}$ to changes in concentration of H1N1 virus was calculated to be − 11.97 % $[\log(TCID50/mL)]^{-1}$ from the slope of the calibration curve (Fig. 4d). The limit of detection (LOD) was calculated to be 9 TCID50/mL using the equation of $LOD = 3\sigma/S$, where σ represents the standard deviation of five measurements containing only the electrolyte and S represents the sensitivity of the sensor [43].

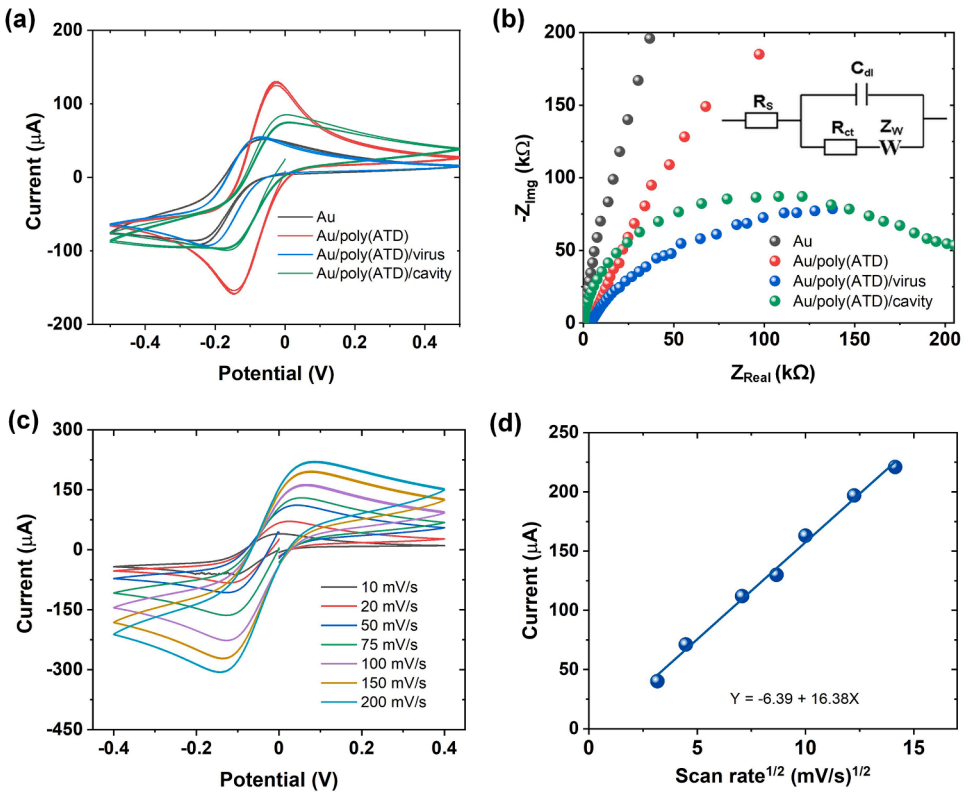

Fig. 3. (a) CV for the bare Au, poly(ATD)/Au, poly(ATD)/Au embedded with virus template, and poly(ATD)/Au with cavities formed after the removal of the virus template. The CV scan was conducted in the electrolyte of 50 mM $[Fe(CN)_6]^{3-/4-}$ in 10 mM Na2SO4 over the potential range from – 0.5–0.5 V at the scan rate of 100 mV/s. (b) Nyquist plots from the EIS scan for the same electrodes tested in (a). (c) CV with different scan rates on the poly(ATD)/Au that contained cavities. Here, RE denotes Ag/AgCl reference electrode. (d) Peak oxidation current as a function of the square root of scan rate.

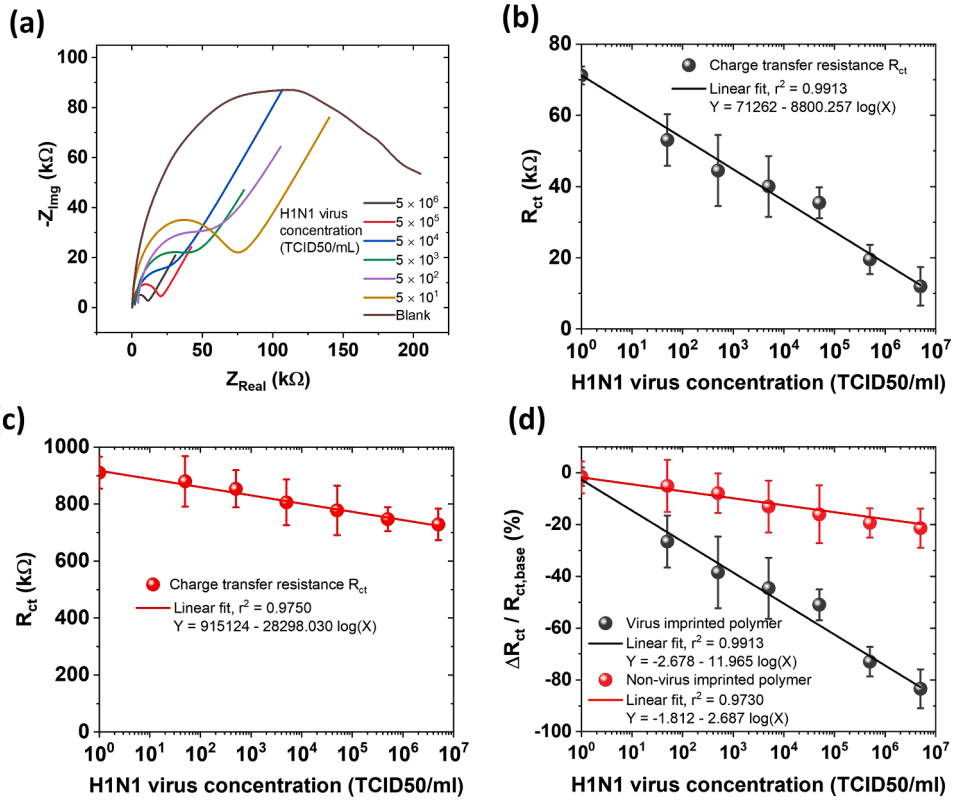

Fig. 4. (a) Nyquist plots obtained from the EIS measurements for H1N1 virus samples with different concentrations. (b) Charge transfer resistance R_{ct} of the VIP sensor as a function of H1N1 virus concentration. (c) R_{ct} value of the NIP device with a non-imprinted polymer of poly(ATD) without cavities. (d) $\Delta R_{ct}/R_{ct,base}$ of the VIP and NIP devices as a function of H1N1 virus concentration. The error bars represent the standard deviation from five repeated measurements.

The cavities of the VIP facilitated specific binding to the IAV H1N1 virus particles. The NIP control device (containing no cavities) was exposed to different concentrations of H1N1 virus. Compared to the VIP sensor, the NIP device exhibited a much lower response of R_{ct} to the presence of H1N1 virus (Fig. 4c), with the sensitivity of $\Delta R_{ct}/R_{ct,base} = -2.69$ % [log(TCID50/mL)]$^{-1}$ (Fig. 4d). Going from 50 TCID50/mL to 5×10^6 TCID50/mL led to only 12 % change in R_{ct} for the NIP sensor while 59 % for the VIP sensor. Therefore, the cavities formed in the VIP resulted in approximately four times enhancement in its response to H1N1 virus compared to the NIP-based counterpart.

Next, the H1N1 virus sensor was exposed to other subtypes of IAV, including H1N2 and H3N2 viruses. The stock virus solution of each subtype here had a concentration of 3.1×10^7 TCID50/mL and was diluted to a range of concentrations in the redox electrolyte. The R_{ct} value of the sensor was found to decrease with increasing concentration of H1N2 or H3N2 virus. The sensitivities of $\Delta R_{ct}/R_{ct,base}$ to H1N2 and H3N2 viruses were calculated to be -5.35 % and -4.65 % [log (TCID50/mL)]$^{-1}$, respectively, based on the slopes of the calibration curves (Fig. 5). This may be because these two subtypes of IAV have similar morphological and functional features to H1N1 virus. Nevertheless, the VIP sensor showed a much higher response when responding to the target H1N1 virus (Fig. 4b) than the non-specific H1N2 and H3N2 viruses (Fig. 5).

To further evaluate the specificity of the sensor, the sensor was exposed to several swine respiratory viral and bacterial pathogens, including *Glaesserella parasuis ((G. parasuis))*, IBV, IDV, *Mycoplasma hyopneumoniae (M. hyopneumoniae)*, PHEV, PRCV, and pseudorabies virus (PRV). The concentration of each interference pathogen in the stock solution was equivalent to that of the H1N1 virus stock (10^7 TCID50/mL). Subsequently, the interference pathogen stock solution was diluted by a factor of two (2X) using the electrolyte solution. The 2X-diluted interference pathogen sample was then applied to the sensor surface. Despite having a similar concentration as the target H1N1 virus, the non-specific pathogens elicited a much lower response from the sensor by 3–16 times, as shown in Fig. 6a. Further, when a high-concentration H1N1 virus sample (5×10^6 TCID50/mL) was spiked with a non-specific pathogen PRRSV or PCV2d (10^5 TCID50/mL each), the R_{ct} value of the sensor was found to decrease by less than 8 % (Fig. 6b). Also, when a low-concentration H1N1 virus sample (5×10^3 TCID50/mL) was spiked with a low-concentration PRRSV or PCV2d (10^3 TCID50/mL each), there occurred a negligibly small change of less than 2 % in the value of R_{ct} Therefore, the sensor was able to detect H1N1 with high selectivity in the presence of these non-specific pathogens.

In addition, the VIP of the sensor could be refreshed with a simple acetic acid wash. To demonstrate this feature, the sensor was first exposed to 5×10^6 TCID50/mL concentration of H1N1 virus. After the EIS measurement was done, the sensor surface was washed with acetic acid (10 % v/v) for 30 min and then cleaned with DI water for another 30 min. The acetic acid solution removed the trapped virus particles from the VIP, thus regenerating active cavities. After the sensor was refreshed, a continuous cycle of virus detection and subsequent surface wash was repeated. Fig. 7 shows that the R_{ct} value of the sensor decreased in response to the virus sample and then recovered to almost the original value after acetic acid wash. After eight cycles, the R_{ct} value still could stay within 88 % of the original value, suggesting that the acetic acid wash is a promising method to refresh and reuse the sensor multiple times.

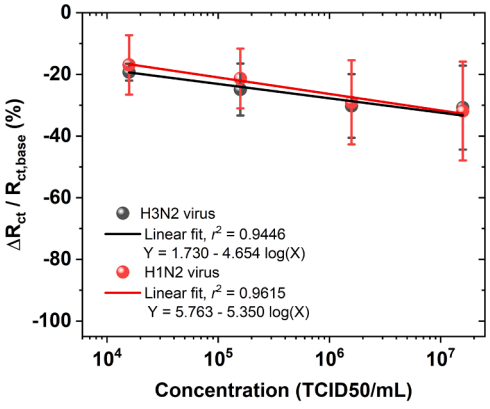

Fig. 5. $\Delta R_{ct}/R_{ct,base}$ of the H1N1 virus sensor when exposed to different concentrations of H1N2 and H3N2 viruses. The error bars represent the standard deviation from five repeated measurements.

The multichannel microfluidic device possessed six identical VIP-based sensing elements specific to H1N1 virus. The device was evaluated for its capability to test multiple samples simultaneously. The experiment began with flowing the pure electrolyte solution into all the measurement chambers through the inlets. The six sensing elements exhibited a low relative standard deviation RSD of 3.8 % from the mean value of R_{ct}. A similar value of RSD was found when the sensing elements were exposed to the same concentration (5×10^3 TCID50/mL) of H1N1 virus. The minor difference in R_{ct} between these elements may be caused by variations in the number of virus particles used while forming the VIP of each element. For the parallel detection, a multichannel syringe pump was used to drive the flows of the six liquid samples and the electrolyte solution from corresponding syringes through the inlets of the microfluidic device. The liquid sample and electrolyte flowed downstream into the passive mixer at the volumetric flow rate ratio of 1:1. The sensing element was immersed in the mixed solution. As mentioned in the Method section, the incubation took one minute, while the EIS measurement required an additional minute. Six swine clinical samples were used to validate the sensor device for parallel testing. These included three IAV PCR-negative samples (one lung tissue homogenate, one nasal swab, and one oral fluid) and three IAV PCR-positive samples (one lung tissue homogenate with Ct 24.6, one nasal swab with Ct 28.1, and one oral fluid with Ct 28.9). For the negative samples, the values of $\Delta R_{ct}/R_{ct,base}$ were found to be within -3 % and the corresponding concentrations were close to zero. In contrast, for the 2X diluted positive samples, the sensors showed a distinct decrease in R_{ct} value (Fig. 8).

4. Conclusions

We have developed and validated a microfluidic electrochemical sensor for the detection of swine H1N1 IAV. Compared to other electrochemical H1N1 virus sensors, our sensor offers a wide dynamic detection range from 50 to 5×10^6 TCID50/mL, a low limit of detection of 9 TCID50/mL, and a short detection time of 2 min, as displayed in Table 1. The VIP of the sensor exhibited remarkable selectivity towards the target virus over a broad range of non-specific bacterial and viral pathogens and demonstrated sustained binding ability to the target virus following multiple washing cycles with acetic acid. VIPs have been combined with various transducers, including those utilizing fluorescence [51–53], surface plasmon resonance [54,55], and quartz crystal microbalance [24] techniques, to detect diverse viral pathogens. Owing to high conductivity, fast electron transfer, and excellent electrocatalytic properties of the poly(APD) material, the VIP-based electrochemical sensor demonstrated remarkable detection performance in terms of limit of detection, detection time, and imprinting factor, as summarized in Table 2. The integration of multiple sensing elements into a microfluidic platform allowed for parallel tests with minimum consumption of samples and reagents. The microfluidic device was demonstrated to rapidly detect swine H1N1 virus in lung homogenates, oral fluids, and nasal swabs. It is worth mentioning that there is much room to improve the microfluidic device. First, different virus species and strains can be detected by creating specific cavities for each target analyte inside the VIP. While the presented sensor has demonstrated a significantly greater response to the target H1N1 virus compared to other subtypes of IAV

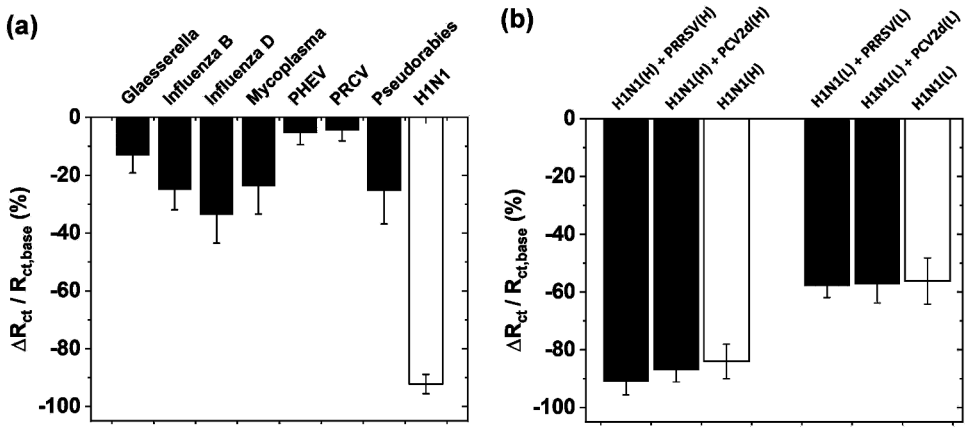

Fig. 6. (a) $\Delta R_{ct}/R_{ct,base}$ of the H1N1 virus sensor when exposed to several swine respiratory viral and bacterial pathogens. The sample of each species used here was diluted two times from its stock solution. (b) Interference test of the H1N1 virus sensor with PRRSV and PCV2d. H1N1(H) denotes the high concentration (5×10^6 TCID50/mL) of H1N1 virus, and H1N1(L) denotes the low concentration (5×10^4 TCID50/mL) of H1N1 virus. The error bars represent the standard deviation of five repeated measurements.

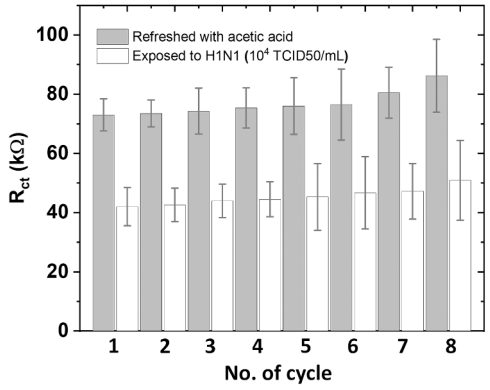

Fig. 7. Regeneration capacity of the VIP for the detection of H1N1 virus. Changes in R_{ct} of the sensor over repeated cycles with each cycle consisting of (i) using acetic acid to remove trapped virus particles and using DI water to clean the sensor surface; (ii) exposing the sensor to the pure electrolyte solution and then the H1N1 virus sample of 10^4 TCID50/mL concentration.

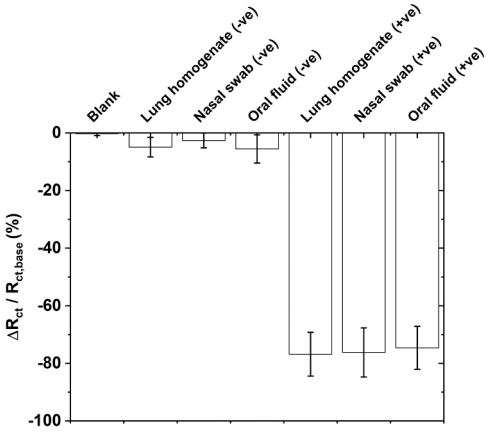

Fig. 8. $\Delta R_{ct}/R_{ct,base}$ of six H1N1 virus sensing elements integrated into the multichannel microfluidic platform. These sensing elements were exposed to the H1N1 negative and positive samples from swine lung homogenates, oral fluids, and nasal swabs. The error bars represent the standard deviation of five repeated measurements.

like H1N2 and H3N2, distinguishing completely between H1N1 and other subtypes of IAV as well as differentiating non-specific subtypes will require substantial efforts. One potential approach to selectively differentiate between various subtypes would involve developing

Table 1
Comparison of the presented sensor with other electrochemical sensors for H1N1 virus.

Detection method	Detection range (TCID50/mL)	Sample volume required (μL)	Limit of detection (TCID50/mL)	Detection time (min)
Differential pulse voltammetry[44]	14 – 1.4×10^4	10	5.2	N/A
Impedance spectroscopy[45]	14 – 1.4×10^6	10 – 20	3	10
Square wave voltammetry[46]	0 – 1.4×10^6	< 20	2.2	< 30
Square wave voltammetry[47]	10 – 10^3	N/A	10	< 30
Differential pulse voltammetry[48]	14 – 1.4×10^4	200	161	30
Impedance spectroscopy[49]	0 – 1.4×10^4	40	4.7	6
Chronoamperometry [50]	1.4 – 1.4×10^4	N/A	0.7	N/A
This work	50 – 5×10^6	12	9	2

separate cavities specific to each subtype in distinct sensing elements, followed by integrating these sensing elements into a single microfluidic device to enable differentiation of all three subtypes. Second, a larger number of sensing elements can be integrated into the microfluidic platform to enable virus detection at higher throughput. In addition, it is possible to integrate low-cost electronic readout circuits and miniature pumps [56] with the microfluidic device to realize a compact, rapid, point-of-care, and multipurpose detection kit for the early detection of pathogens. Given the recent COVID-19 pandemic, the sensor can be adapted to detect SARS-CoV-2 virus by substituting H1N1 IAV with SARS-CoV-2 virus particles during the electropolymerization of corresponding VIP materials. Promising studies have shown the potential of the VIP strategy for detecting SARS-CoV-2 virus. However, it is crucial to conduct comprehensive sensor characterizations to evaluate the sensor's performance in the presence of various interfering pathogens. Additionally, further research is necessary to scale up the production of VIP-based sensors, and to optimize conducting polymers for developing cavities that are specific to SARS-CoV-2 virus [57–59].

CRediT authorship contribution statement

Raufur Rahman Khan: Methodology, Validation, Analysis, Writing – original draft. **Hussam Ibrahim**: Methodology, Validation, Analysis. **Gaurav Rawal**: Methodology, Validation, Resources. **Jianqiang Zhang:** Methodology, Validation, Resources, Analysis, Supervision, Funding acquisition. **Meng Lu:** Methodology, Validation, Resources,

Table 2
Comparison of the presented sensor with other VIP-based non-electrochemical sensors for various viral pathogens.

Method of transduction	Monomer	Target analyte	Limit of detection[a]	Detection time (min)	Imprinting factor
Fluorescence[51]	(3-aminopropyl)triethoxysilane	Japanese encephalitis virus against HAV, Leprosy virus (LV), and Rabies virus (RV)	9.6 pM	40	2.12
Fluorescence[52]	(3-aminopropyl)triethoxysilane	JEV against LV and RV	0.32 nM	N/A	2.98
Fluorescence[53]	(3-aminopropyl)triethoxysilane	JEV against simian virus, HAV, RV	0.11 pM	55	1.7
Surface plasmon resonance[54]	Acrylamide, N-t-butylacrylamide, 2-hydroxyethyl methacrylate, N,N'-methylene bisacrylamide	SARS-CoV-2 against MERS-CoV spike protein	580 nM	10	N/A
Surface plasmon resonance[55]	N-isopropylacrylamide, N,N'-methylene-bis-acrylamide, N-tert-butylacryamide, acrylic acid	Bacteriophage MS2	7.1×10^6 TCID50/mL	240	N/A
Quartz crystal microbalance[24]	Acrylamide, Methacrylic acid, methylmethacrylate, N-vinylpyrrolidone	H5N1, H5N3, H1N1, H1N3, H6N1 against each other	10^5 TCID50/mL	40	N/A
This work	2-Amino-1,3,4-thiadiazole	H1N1 against H1N2, H3N2, IBV, IDV, PHEV, PRCV, PRV, M. *hyopneumoniae*, G. *parasuis*	9 TCID50/mL	2	4[b]

[a] The limit of detection values given in references [51–54] use the unit mole per liter, which considers the number of viral particles in the sample. On the other hand, TCID50 measures the dilution of the virus needed to infect 50 % of the cell culture wells. Therefore, it is not suitable to convert from mole per liter to TCID50/mL.
[b] The imprinting factor can be described as the proportion of the sensing signal obtained from the device utilizing VIP compared to NIP at a virus concentration of 10^7 TCID50/mL (as shown in Fig. 4d).

Analysis, Funding acquisition. **Liang Dong:** Conceptualization, Methodology, Validation, Resources, Analysis, Supervision, Funding acquisition, Writing – original draft, Writing – review & editing.

Declaration of Competing Interest

The authors declare that they have no known competing financial interests or personal relationships that could have appeared to influence the work reported in this paper.

Data availability

Data will be made available on request.

Acknowledgment

This work was supported by Iowa State University's COVID-19 Seed Grant. The authors thank Yang Tian for his help with e-beam evaporation.

References

[1] T. Norton, C. Chen, M.L.V. Larsen, D. Berckmans, Precision livestock farming: building 'digital representations' to bring the animals closer to the farmer, Animal 13 (12) (2019) 3009–3017.
[2] J. Vidic, M. Manzano, C.M. Chang, N. Jaffrezic-Renault, Advanced biosensors for detection of pathogens related to livestock and poultry, Vet. Res. 48 (1) (2017) 1–22.
[3] K. VanderWaal, J. Deen, Global trends in infectious diseases of swine, Proc. Natl. Acad. Sci. USA 115 (45) (2018) 11495–11500.
[4] A. Vincent, L. Awada, I. Brown, H. Chen, F. Claes, G. Dauphin, R. Donis, M. Culhane, K. Hamilton, N. Lewis, E. Mumford, Review of influenza A virus in swine worldwide: a call for increased surveillance and research, Zoonoses Public Health 61 (1) (2014) 4–17.
[5] P.R. Saunders-Hastings, D. Krewski, Reviewing the history of pandemic influenza: understanding patterns of emergence and transmission, Pathogens 5 (4) (2016) 66.
[6] R. Dhumpa, K.J. Handberg, P.H. Jørgensen, S. Yi, A. Wolff, D.D. Bang, Rapid detection of avian influenza virus in chicken fecal samples by immunomagnetic capture reverse transcriptase–polymerase chain reaction assay, Diagn. Microbiol. Infect. Dis. 69 (3) (2011) 258–265.
[7] Q. Yuan, X.D. Cheng, B.C. Yang, Q.B. Zheng, Y.X. Chen, Q.R. Chen, F. Zeng, R. Zhang, S.X. Ge, X.K. Hao, H. Chen, Differential diagnosis of pandemic (H1N1) 2009 infection by detection of haemagglutinin with an enzyme-linked immunoassay, Clin. Microbiol. Infect. 17 (10) (2011) 1574–1580.
[8] Y. Ji, W. Guo, L. Zhao, H. Li, G. Lu, Z. Wang, G. Wang, C. Liu, W. Xiang, Development of an antigen-capture ELISA for the detection of equine influenza virus nucleoprotein, J. Virol. Methods 175 (1) (2011) 120–124.
[9] Q. He, K.H. Chong, H.H. Chng, B. Leung, A.E. Ling, T. Wei, S.W. Chan, E.E. Ooi, J. Kwang, Development of a Western blot assay for detection of antibodies against coronavirus causing severe acute respiratory syndrome, Clin. Vaccin. Immunol. 11 (2) (2004) 417–422.
[10] M. Onno, A. Jestin, P. Vannier, C. Kaiser, Diagnosis of swine influenza with an immunofluorescence technique using monoclonal antibodies, Vet. Q. 12 (4) (1990) 251–254.
[11] N. Chauhan, J. Narang, S. Pundir, S. Singh, C.S. Pundir, Laboratory diagnosis of swine flu: a review, Artif. Cells, Nanomed., Biotechnol. 41 (3) (2013) 189–195.
[12] Q. Zhang, G. Rawal, J. Qian, H. Ibrahim, J. Zhang, L. Dong, M. Lu, An integrated magneto-opto-fluidic biosensor for rapid on-chip assay of respiratory viruses of livestock, Lab Chip 22 (17) (2022) 3236–3244.
[13] L. Chen, Z. Sheng, A. Zhang, X. Guo, J. Li, H. Han, M. Jin, Quantum-dots-based fluoroimmunoassay for the rapid and sensitive detection of avian influenza virus subtype H5N1, Luminescence 25 (6) (2010) 419–423.
[14] L. Wang, J. Tian, W. Yang, Y. Zhao, S. Zhao, A T7exonuclease-assisted target recycling amplification with graphene oxide acting as the signal amplifier for fluorescence polarization detection of human immunodeficiency virus (HIV) DNA, Luminescence 31 (2) (2016) 573–579.
[15] D. Su, K. Wu, V.D. Krishna, T. Klein, J. Liu, Y. Feng, A.M. Perez, M.C.J. Cheeran, J. P. Wang, Detection of influenza a virus in swine nasal swab samples with a wash-free magnetic bioassay and a handheld giant magnetoresistance sensing system, Front. Microbiol. 10 (2019) 1077.
[16] C.E. Nilsson, S. Abbas, M. Bennemo, A. Larsson, M.D. Hämäläinen, Å. Frostell-Karlsson, A novel assay for influenza virus quantification using surface plasmon resonance, Vaccine 28 (3) (2010) 759–766.
[17] K. Kiilerich-Pedersen, J. Daprà, S. Cherré, N. Rozlosnik, High sensitivity point-of-care device for direct virus diagnostics, Biosens. Bioelectron. 49 (2013) 374–379.
[18] T. Matsubara, M. Ujie, T. Yamamoto, M. Akahori, Y. Einaga, T. Sato, Highly sensitive detection of influenza virus by boron-doped diamond electrode terminated with sialic acid-mimic peptide, Proc. Natl. Acad. Sci. USA 113 (32) (2016) 8981–8984.
[19] H. Zhang, B.L. Miller, Immunosensor-based label-free and multiplex detection of influenza viruses: state of the art, Biosens. Bioelectron. 141 (2019), 111476.
[20] W. Liu, Y. Ma, G. Sun, S. Wang, J. Deng, H. Wei, Molecularly imprinted polymers on graphene oxide surface for EIS sensing of testosterone, Biosens. Bioelectron. 92 (2017) 305–312.
[21] H. da Silva, J.G. Pacheco, J.M. Magalhães, S. Viswanathan, C. Delerue-Matos, MIP-graphene-modified glassy carbon electrode for the determination of trimethoprim, Biosens. Bioelectron. 52 (2014) 56–61.
[22] L. Andersson, B. Sellergren, K. Mosbach, Imprinting of amino acid derivatives in macroporous polymers, Tetrahedron Lett. 25 (45) (1984) 5211–5214.
[23] J.J. BelBruno, Molecularly imprinted polymers, Chem. Rev. 119 (1) (2018) 94–119.
[24] T. Wangchareansak, A. Thitithanyanont, D. Chuakheaw, M.P. Gleeson, P. A. Lieberzeit, C. Sangma, Influenza A virus molecularly imprinted polymers and their application in virus sub-type classification, J. Mater. Chem. B 1 (16) (2013) 2190–2197.
[25] T. Wangchareansak, A. Thitithanyanont, D. Chuakheaw, M.P. Gleeson, P. A. Lieberzeit, C. Sangma, A novel approach to identify molecular binding to the influenza virus H5N1: screening using molecularly imprinted polymers (MIPs), MedChemComm 5 (5) (2014) 617–621.
[26] C. Tancharoen, W. Sukjee, C. Thepparit, T. Jaimipuk, P. Auewarakul, A. Thitithanyanont, C. Sangma, Electrochemical biosensor based on surface imprinting for zika virus detection in serum, ACS Sens. 4 (1) (2018) 69–75.
[27] J.A. Arter, D.K. Taggart, T.M. McIntire, R.M. Penner, G.A. Weiss, Virus-PEDOT nanowires for biosensing, Nano Lett. 10 (12) (2010) 4858–4862.
[28] K.C. Donavan, J.A. Arter, R. Pilolli, N. Cioffi, G.A. Weiss, R.M. Penner, Virus− poly (3, 4-ethylenedioxythiophene) composite films for impedance-based biosensing, Anal. Chem. 83 (7) (2011) 2420–2424.
[29] W.M. Yeh, K.C. Ho, Amperometric morphine sensing using a molecularly imprinted polymer-modified electrode, Anal. Chim. Acta 542 (1) (2005) 76–82.
[30] A. Raziq, A. Kidakova, R. Borozjak, J. Reut, A. Öpik, V. Syritski, Development of a portable MIP-based electrochemical sensor for detection of SARS-CoV-2 antigen, Biosens. Bioelectron. 178 (2021), 113029.

[31] Z. Altintas, M. Gittens, A. Guerreiro, K.A. Thompson, J. Walker, S. Piletsky, I. E. Tothill, Detection of waterborne viruses using high affinity molecularly imprinted polymers, Anal. Chem. 87 (13) (2015) 6801–6807.
[32] G.J. Soufi, S. Iravani, R.S. Varma, Molecularly imprinted polymers for the detection of viruses: challenges and opportunities, Analyst 146 (10) (2021) 3087–3100.
[33] M.S. Amorim, M.G.F. Sales, M.F. Frasco, Recent advances in virus imprinted polymers, Biosens. Bioelectron.: X (2022), 100131.
[34] S.A. Zaidi, An overview of bio-inspired intelligent imprinted polymers for virus determination, Biosensors 11 (3) (2021) 89.
[35] R.H. Liu, M.A. Stremler, K.V. Sharp, M.G. Olsen, J.G. Santiago, R.J. Adrian, H. Aref, D.J. Beebe, Passive mixing in a three-dimensional serpentine microchannel, J. Micro Syst. 9 (2) (2000) 190–197.
[36] H. Ibrahim, S. Moru, P. Schnable, L. Dong, Wearable plant sensor for In situ monitoring of volatile organic compound emissions from crops, ACS Sens. 7 (8) (2022) 2293–2302.
[37] C.W. Kellett, W.B. Swords, M.D. Turlington, G.J. Meyer, C.P. Berlinguette, Resolving orbital pathways for intermolecular electron transfer, Nat. Commun. 9 (1) (2018) 4916.
[38] J. Zhang, P.C. Gauger, Isolation of swine influenza A virus in cell cultures and embryonated chicken eggs, Methods Mol. Biol. 2123 (2020) 281–294.
[39] J. Zhang, K.M. Harmon, RNA extraction from swine samples and detection of influenza A virus in swine by real-time RT-PCR. Animal Influenza Virus, Humana Press, New York, NY, 2014, pp. 277–293.
[40] Z. Xu, X. Wang, R.J. Weber, R. Kumar, L. Dong, Nutrient sensing using chip scale electrophoresis and in situ soil solution extraction, IEEE Sens. J. 17 (14) (2017) 4330–4339.
[41] M.A. Ali, W. Hong, S. Oren, Q. Wang, Y. Wang, H. Jiang, L. Dong, Tunable bioelectrodes with wrinkled-ridged graphene oxide surfaces for electrochemical nitrate sensors, RSC Adv. 6 (71) (2016) 67184–67195.
[42] H. Jiang, M. Ali, Z. Xu, L.J. Halverson, L. Dong, Integrated microfluidic flow-through microbial fuel cells, Sci. Rep. 7 (1) (2017) 1–12.
[43] Y. Wang, Q. Zhang, W. Yuan, Y. Wang, H.J. Loghry, Z. Zhao, M.J. Kimber, L. Dong, M. Lu, Hyperspectral imaging-based exosome microarray for rapid molecular profiling of extracellular vesicles, Lab Chip 21 (1) (2021) 196–204.
[44] J. Bhardwaj, N. Chaudhary, H. Kim, J. Jang, Subtyping of influenza A H1N1 virus using a label-free electrochemical biosensor based on the DNA aptamer targeting the stem region of HA protein, Anal. Chim. Acta 1064 (2019) 94–103.
[45] J. Bhardwaj, M.W. Kim, J. Jang, Rapid airborne influenza virus quantification using an antibody-based electrochemical paper sensor and electrostatic particle concentrator, Environ. Sci. Technol. 54 (17) (2020) 10700–10712.
[46] J.H. Kim, J.H. Shin, C.H. Cho, J. Hwang, D.H. Kweon, T.J. Park, C.H. Choi, J. P. Park, Dual synergistic response for the electrochemical detection of H1N1 virus and viral proteins using high affinity peptide receptors, Talanta (2022), 123613.
[47] B.S. Ferguson, S.F. Buchsbaum, T.T. Wu, K. Hsieh, Y. Xiao, R. Sun, H.T. Soh, Genetic analysis of H1N1 influenza virus from throat swab samples in a microfluidic system for point-of-care diagnostics, J. Am. Chem. Soc. 133 (23) (2011) 9129–9135.
[48] S. Devarakonda, R. Singh, J. Bhardwaj, J. Jang, Cost-effective and handmade paper-based immunosensing device for electrochemical detection of influenza virus, Sensors 17 (11) (2017) 2597.
[49] J. Bhardwaj, A. Sharma, J. Jang, Vertical flow-based paper immunosensor for rapid electrochemical and colorimetric detection of influenza virus using a different pore size sample pad, Biosens. Bioelectron. 126 (2019) 36–43.
[50] R. Singh, S. Hong, J. Jang, Label-free detection of influenza viruses using a reduced graphene oxide-based electrochemical immunosensor integrated with a microfluidic platform, Sci. Rep. 7 (1) (2017) 1–11.
[51] C. Liang, H. Wang, K. He, C. Chen, X. Chen, H. Gong, C. Cai, A virus-MIPs fluorescent sensor based on FRET for highly sensitive detection of JEV, Talanta 160 (2016) 360–366.
[52] K. He, C. Chen, C. Liang, C. Liu, B. Yang, X. Chen, C. Cai, Highly selective recognition and fluorescent detection of JEV via virus-imprinted magnetic silicon microspheres, Sens. Actuators B: Chem. 233 (2016) 607–614.
[53] W. Feng, C. Liang, H. Gong, C. Cai, Sensitive detection of Japanese encephalitis virus by surface molecularly imprinted technique based on fluorescent method, N. J. Chem. 42 (5) (2018) 3503–3508.
[54] N. Cennamo, G. D'Agostino, C. Perri, F. Arcadio, G. Chiaretti, E.M. Parisio, G. Camarlinghi, C. Vettori, F. Di Marzo, R. Cennamo, G. Porto, Proof of concept for a quick and highly sensitive on-site detection of SARS-CoV-2 by plasmonic optical fibers and molecularly imprinted polymers, Sensors 21 (5) (2021) 1681.
[55] Z. Altintas, M. Gittens, A. Guerreiro, K.A. Thompson, J. Walker, S. Piletsky, I. E. Tothill, Detection of waterborne viruses using high affinity molecularly imprinted polymers, Anal. Chem. 87 (13) (2015) 6801–6807.
[56] X. Wang, H. Jiang, Y. Chen, X. Qiao, L. Dong, Microblower-based microfluidic pump, Sens. Actuators A: Phys. 253 (2017) 27–34.
[57] A.G. Ayankojo, R. Boroznjak, J. Reut, A. Öpik, V. Syritski, Molecularly imprinted polymer based electrochemical sensor for quantitative detection of SARS-CoV-2 spike protein, Sens. Actuators B: Chem. 353 (2022), 131160.
[58] M.A. Tabrizi, J.P. Fernández-Blázquez, D.M. Medina, P. Acedo, An ultrasensitive molecularly imprinted polymer-based electrochemical sensor for the determination of SARS-CoV-2-RBD by using macroporous gold screen-printed electrode, Biosens. Bioelectron. 196 (2022), 113729.
[59] A. Raziq, A. Kidakova, R. Boroznjak, J. Reut, A. Öpik, V. Syritski, Development of a portable MIP-based electrochemical sensor for detection of SARS-CoV-2 antigen, Biosens. Bioelectron. 178 (2021), 113029.

Raufur Rahman Khan is a Ph.D. graduate student in the Department of Electrical and Computer Engineering at Iowa State University (Ames, Iowa, USA). His research focuses on biosensors, semiconductors, and memristors.

Hussam Ibrahim obtained his B.S. in Physics and Applied Mathematics from Augustana College (Rock Island, Illinois, USA) in 2017 and Ph.D. in Electrical Engineering at Iowa State University (Ames, Iowa, USA) in 2022. He presently works as a semiconductor process engineer with VueReal Inc. (Waterloo, Ontario, Canada).

Gaurav Rawal is a graduate student in the Department of Veterinary Diagnostic and Production Animal Medicine at Iowa State University (Ames, Iowa, USA). He received his DVM from Nepal in 2014 and MS from Iowa State in Veterinary Preventive Medicine in 2019. He is pursuing his Ph.D. with a focus on applied virology and PRRS vaccine immunology.

Jianqiang Zhang is a professor in the Department of Veterinary Diagnostic and Production Animal Medicine at Iowa State University (Ames, Iowa, USA). He obtained his M.D. from Beijing Medical University (Beijing, China) in 1996, M.S. in Molecular Virology from Institute of Virology, Chinese Academy of Preventive Medicine (Beijing, China) in 1999, and Ph.D. in Veterinary Science (Molecular Virology) from University of Kentucky (Lexington, KY, USA) in 2005. His research interests include virus diagnostic assay development and validation, investigational disease outbreaks and molecular characterization of viruses, virus-host cell interactions, application of reverse genetics system in the study of virus pathogenesis, and vaccine development.

Meng Lu is an associate professor in the Department of Electrical and Computer Engineering and the Department of Mechanical Engineering at Iowa State University (Ames, Iowa, USA). He obtained his Ph.D. and M.S. from the University of Illinois at Urbana Champaign (Illinois, USA) in 2008 and 2005, respectively, and B.S. from the University of Science and Technology of China (Anhui, China) in 2002. His research interests are optical sensors for chemical and biological analysis, photonic devices, microfluidics for sensor integration and optical instrumentation. He received the National Science Foundation CAREER Award.

Liang Dong is currently the Vikram Dalal Professor in the Department of Electrical and Computer Engineering at Iowa State University (Ames, Iowa, USA). He is also the Director of the Microelectronics Research Center and the Faculty Scholar of the Plant Sciences Institute at Iowa State. He previously worked as a Postdoctoral Research Associate in the Department of Electrical and Computer Engineering at the University of Wisconsin-Madison. He received his Ph.D. in Electronic Science and Technology at Tsinghua University (Beijing, China). His research interests include MEMS/NEMS, sensors, optical devices, microfluidic devices, and micro/nanoscale manufacturing, and their applications in sustainable agriculture and environments, plant science, biomedicine, and the Internet of Things. He received the National Science Foundation CAREER Award. He has served as Editor-in-Chief of Sensors and Actuators A: Physical since 2018.